

Taper-induced control of viscous fingering in variable-gap Hele-Shaw flows

Eduardo O. Dias and José A. Miranda*

Departamento de Física, Universidade Federal de Pernambuco, Recife, PE 50670-901, Brazil

(Received 18 March 2013; published 22 May 2013)

Variable-gap Hele-Shaw flows consider viscous fluid displacements resulting from the lifting or squeezing of the upper cell plate, while the lower plate remains at rest. Conventionally, researchers focus on the situation in which the cell plates are perfectly parallel. We study a slightly different version of the problem, where the upper plate is gently inclined so that the plates are no longer parallel. Within this tapered Hele-Shaw cell context we examine how the presence of such a small gap gradient affects the stability properties of the fluid-fluid interface. Linear stability analysis indicates that the existence of the taper offers a simple geometric way to control the development of interfacial fingering instabilities under both lifting and squeeze flow circumstances.

DOI: [10.1103/PhysRevE.87.053015](https://doi.org/10.1103/PhysRevE.87.053015)

PACS number(s): 47.15.gp, 47.20.Ma, 68.35.Np, 68.15.+e

I. INTRODUCTION

The lifting Hele-Shaw flow is a variant of the conventional, constant gap spacing Saffman-Taylor problem [1–3]. It provides an alternative way to produce viscous fingering patterns by stretching a very thin layer of a viscous fluid, sandwiched between two parallel plates of a Hele-Shaw cell. This is done by lifting the upper plate while the lower one remains at rest. As the plates separate, the outer less viscous fluid enters the system, and the more viscous inner fluid moves inward to conserve volume. As a result, the fluid-fluid interface deforms, forming complex, visually striking patterns [4–17].

The reverse flow situation is accomplished by compressing the upper plate of the Hele-Shaw cell, so that the more viscous inner fluid pushes the less viscous outer one. This characterizes a fluid displacement arrangement commonly known as squeeze flow [18,19]. In this case the flow is stable, meaning that the fluid-fluid boundary is nearly circular, and interfacial instabilities are damped out.

In addition to being an intrinsically important academic problem, the variable-gap Hele-Shaw cell system is also intimately related to the practical problem of adhesion [17–33]. In such types of problems the force and the energy required to separate two adhesively bonded surfaces can be quite successfully evaluated through the so-called probe-tack test [34,35], which essentially employs a lifting Hele-Shaw setup.

Despite the rich morphology and dynamics of the radial patterns produced by variable-gap Hele-Shaw flows, in some practical circumstances such as in adhesion science the formation of convoluted interfacial shapes is undesirable. In fact, it has been verified both theoretically and experimentally that the fingering formation process is indeed responsible for the decrease in the adhesion force [13,17,22]. This suggests that one could regulate the adhesive strength of confined fluids by favoring or restraining the development of fingering patterns. Therefore, one key aspect of both scientific and practical points of view is to be able to precisely control the rising of fingering structures in variable-gap confined flows.

In this work we introduce a small modification to the traditional parallel plate setup used in existing lifting and squeeze Hele-Shaw flow investigations. We consider a tapered

Hele-Shaw geometry [36,37] in which the moving upper plate is inclined a little bit in such a way that the cell presents a small, constant depth gradient along the radial direction. This is done while keeping the lower cell plate flat and motionless (see Fig. 1). In this context, a lifting or squeezing process can take place as in common variable-gap Hele-Shaw circumstances, but now the cell plates are not exactly parallel. In this framework the small gap gradient can be either positive [slowly diverging plates; Fig. 1(a)] or negative [slowly converging plates; Fig. 1(b)].

Our study is motivated by the recent success of the gap gradient strategy in offering opportunities to tune fingering behavior in the traditional Saffman-Taylor problem with motionless parallel plates [38–41], as well as in the rotating Hele-Shaw problem [42]. We examine how the sign and magnitude of the small gap gradient affect the stability of the interface for variable-gap Hele-Shaw processes. Our ultimate goal is to devise a simple way, based on the geometry of the Hele-Shaw cell configuration, to inhibit the viscous fingering instability for lifting flows and stimulate it under squeeze flow displacements.

II. BASIC EQUATIONS AND LINEAR STABILITY CALCULATION

Consider a fluid of viscosity η surrounded by an inviscid fluid sandwiched in the confined geometry of a tapered Hele-Shaw cell (see Fig. 1). The fluids are incompressible, and there exists a nonzero surface tension σ between them. In contrast to the conventional parallel plate setup, the upper cell plate has a constant small depth gradient b' ($|b'| \ll 1$) in the radial direction. This plate is allowed to move up (lifting flow) or down (squeeze flow) along the z axis, which is perpendicular to the lower cell plate. The lower plate is held fixed at $z = 0$. The coordinate system is defined in such a way that its origin is located at the center of the cell. In these conditions, the cell gap can be written as $b(r, t) = b_0(t) + b'r$, where $b_0(t)$ is the time varying cell spacing at its center.

During the upper plate lifting process, the initially unperturbed, circular interface can become unstable and deform due to the interplay of viscous and capillary forces. Therefore, we express the interface as $\mathcal{R}(\theta, t) = R(t) + \zeta(\theta, t)$, where $R(t)$ is the time-dependent unperturbed radius of the interface and $\zeta(\theta, t)$ represents the net interface disturbance. Given a

*jme@df.ufpe.br

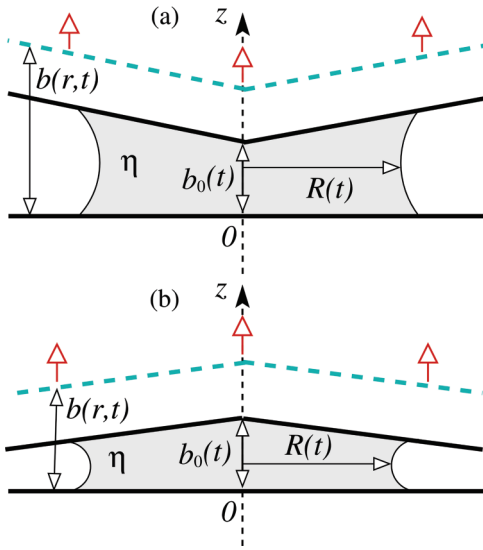


FIG. 1. (Color online) Schematic representation (side view) of a radially tapered variable-gap Hele-Shaw cell, presenting (a) a positive and (b) a negative gap gradient. Here we illustrate the case of lifting flow, where the upper plate (represented by the thick dashed lines) is pulled upward. The viscous fluid (viscosity η) is depicted in gray, and the varying cell gap width is denoted as $b(r,t)$. $R(t)$ represents the time-dependent radius of the unperturbed fluid-fluid interface.

time-dependent variable-gap profile function $b_0(t)$, conservation of volume leads to a useful relation that is expressed, as $R(t)$ evolves in time, as

$$\frac{2b'}{3}R^3(0) + R^2(0)b_0(0) = \frac{2b'}{3}R^3(t) + R^2(t)b_0(t). \quad (1)$$

In addition, we rewrite the variable cell gap as a function of $R(t)$,

$$b(r,t) = b_i(t) + b'[r - R(t)], \quad (2)$$

where $b_i(t) = b_0(t) + b'R(t)$ is the cell spacing at $r = R(t)$. Here r denotes the radial coordinate and varies from zero to infinity. However, to cover the entire inner fluid we have that $0 \leq r \leq \mathcal{R}$.

The basic hydrodynamic equation of the problem is Darcy's law,

$$\mathbf{v} = -\frac{b^2(r,t)}{12\eta} \nabla P, \quad (3)$$

where $\mathbf{v} = \mathbf{v}(r,\theta)$ and $P = P(r,\theta)$ are the gap-averaged velocity and pressure, respectively. Here θ denotes the polar angle in the r - θ plane.

The incompressibility condition for the smoothly varying gap situation is given by [36,37,43]

$$\nabla \cdot [b(r,t)\mathbf{v}] = -\dot{b}(r,t), \quad (4)$$

with $\dot{b}(r,t) = \dot{b}_0(t)$. From now on, since we are interested in the onset of the interfacial instability and $|b'| \ll 1$, we consider that $3b'[r - R(t)]/b_i(t) \ll 1$ [36]. Substituting Eq. (3) into Eq. (4), we obtain a partial differential equation for the pressure,

$$\nabla^2 P + \frac{3b'}{b_i(t)} \frac{\partial P}{\partial r} - \frac{12\eta\dot{b}_0(t)}{b_i^3(t)} = 0. \quad (5)$$

The most general solution of Eq. (5) can be written as [37,43]

$$P(r,\theta) = f(r) + g(r)e^{in\theta}. \quad (6)$$

Substituting Eq. (6) into Eq. (5), we have

$$\frac{1}{r} \frac{d}{dr} \left(r \frac{df}{dr} \right) + \frac{3b'}{b_i(t)} \frac{df}{dr} - \frac{12\eta\dot{b}_0(t)}{b_i^3(t)} = 0 \quad (7)$$

and

$$\frac{1}{r} \frac{d}{dr} \left(r \frac{dg}{dr} \right) + \frac{3b'}{b_i(t)} \frac{dg}{dr} - \frac{n^2}{r^2} g(r) = 0. \quad (8)$$

By taking into consideration that $3b'[r - R(t)]/b_i(t) \ll 1$, the solution of $f(r)$ is given by

$$f(r) = \frac{12\eta\dot{b}_0(t)}{b_i^3(t)} \frac{r^2}{4}. \quad (9)$$

In the limit of parallel Hele-Shaw plates ($b' = 0$), $b_i(t) = b_0(t)$, and this solution reproduces the results obtained in [4]. On the other hand, the solution for $g(r)$ is

$$g(r) = \sum_n P_n(t) r^{|n|} \Phi(|n|, 1 + 2|n|; -3b'r/b_i(t)) e^{in\theta}, \quad (10)$$

where $\Phi(|n|, 1 + 2|n|; -3b'r/b_i(t))$ is the Kummer confluent hypergeometric function [44],

$$\Phi(a,b;z) = \sum_{k=0}^{\infty} \frac{(a)_k z^k}{(b)_k k!}, \quad (11)$$

and $(x)_k = x(x+1)(x+2)\dots(x+k-1)$. The function $\Phi(a,b;z)$ is also known as the confluent hypergeometric function of the first kind ${}_1F_1(a,b;z)$, being a degenerate form of the hypergeometric function ${}_2F_1(a,b,c;z)$, which arises as a solution to the confluent hypergeometric differential equation [45].

At this point, we have the elements needed to perform a linear stability analysis of the system. We begin by describing the net interface perturbation $\zeta(\theta,t) = \sum_{n \neq 0} \zeta_n(t) \exp(in\theta)$ with Fourier amplitudes $\zeta_n(t)$ and discrete wave numbers n . To find a relation between $P_n(t)$ in Eq. (10) and $\zeta_n(t)$, we consider the kinematic boundary condition [2], which states that the normal components of fluid velocity at the interface equal the velocity of the interface itself,

$$\frac{\partial \mathcal{R}}{\partial t} = \left(v_r - \frac{1}{r} \frac{\partial \zeta}{\partial \theta} v_\theta \right)_{r=\mathcal{R}}, \quad (12)$$

where v_r and v_θ are the components of the depth-averaged velocity \mathbf{v} . We keep terms up to first order in the parameter ζ and then Fourier transform. Solving for $P_n(t)$ consistently yields

$$P_n(t) = \frac{12\eta}{b_i^2(t)} \frac{R(t)}{[R(t)]^{|n|} |n| \Phi_1} \times \left[1 - \frac{3b'R(t)}{b_i(t)} \frac{1}{(1+2|n|) \Phi_1} \Phi_2 \right]^{-1} \times \left\{ -\dot{\zeta}_n - \left(\frac{\dot{b}_0(t)}{2b_i(t)} + \frac{b'R(t)\dot{b}_0(t)}{b_i^2(t)} \right) \zeta_n \right\}, \quad (13)$$

where the overdot denotes the total time derivative, $\Phi_1 = \Phi(|n|, 1 + 2|n|; -3b'R(t)/b_i(t))$, and $\Phi_2 = \Phi(1 + |n|, 2 + 2|n|; -3b'R(t)/b_i(t))$. Notice that the product $3b'R(t)/b_i(t)$ is not necessarily small since the ratio $R(t)/b_i(t)$ can be large.

Another important boundary condition is the pressure jump at the interface [1,2], which is given by the Young-Laplace equation

$$P(r = \mathcal{R}, \theta) = \left(\sigma \kappa + \frac{2\sigma \cos \beta}{b(r,t)} \right)_{r=\mathcal{R}}. \quad (14)$$

In Eq. (14) κ denotes the interface curvature in the plane of the cell. On the other hand, the term proportional to $1/b(r,t)$ is associated with the curvature for the direction across the gap, and β is the static contact angle measured between the plates and the curved fluid meniscus. As in Refs. [38,41] we focus on the $\beta = \pi$ situation, when the viscous fluid is said to be wetting. We point out that the relevant three-dimensional contribution of the contact angle β has not been taken into account in the conventional lifting Hele-Shaw flow studies presented in Refs. [4–17].

Hereafter, we consider the upper plate velocity as a constant function in time, $\dot{b}_0(t) = \dot{b}$, which can assume positive (lifting flow) or negative (squeeze flow) values. Moreover, we work with the dimensionless version of the equations so that transversal and parallel lengths to the cell plane are rescaled by $b_i(0)$ and $R(0)$, respectively. Time is rescaled by $b_i(0)/|\dot{b}|$. Note that in the dimensionless version of the equations the parameter $3b'\delta\zeta/b_i(t) \ll 1$, where $\delta = R(0)/b_i(0)$ represents the aspect ratio of the circular blob at time $t = 0$.

To obtain the equation of motion for the perturbation amplitude $\zeta_n(t)$, first we substitute Eq. (13) into Eq. (10) evaluated at the interface. Then, we insert the resulting expression plus the solution for $f(r)$ [Eq. (9)] into Eq. (6). Finally, we match the expression for this pressure field with the Young-Laplace condition (14) to get the equation of motion. Keeping terms up to the first order in ζ and Fourier transforming, we obtain

$$\dot{\zeta}_n = \lambda(n)\zeta_n, \quad (15)$$

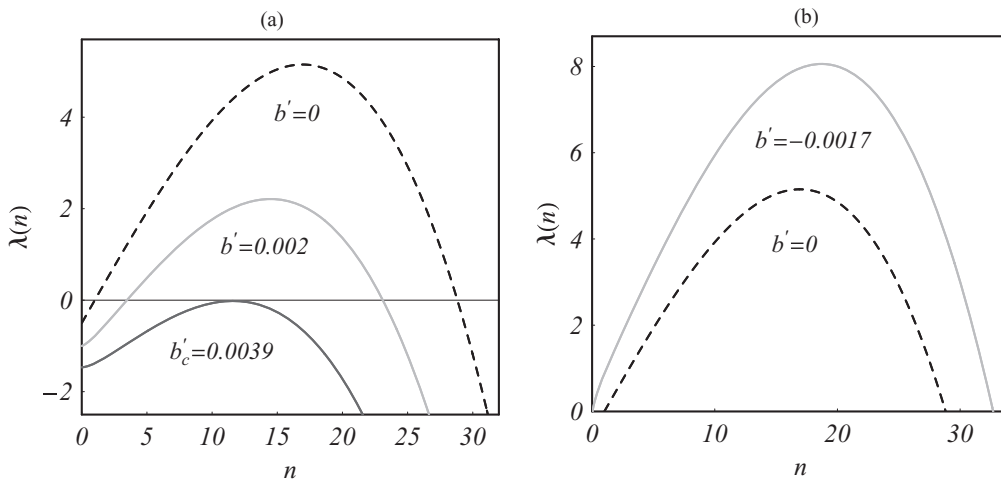


FIG. 2. Linear growth rate $\lambda(n)$ as a function of n for $\text{Ca} = 1.1 \times 10^{-4}$ and $\delta = 250$: (a) $b' = 0$ (dashed curve), $b' = 0.002$ (light gray curve), and $b' = b'_c = 0.0039$ (dark gray curve); (b) $b' = 0$ (dashed curve), $b' = -0.0017$ (gray curve).

where

$$\begin{aligned} \lambda(n) = & \frac{\pm 1}{2b_i(t)} (|n| - 1) - \frac{b_i^2(t)}{[R(t)\delta]^3} \frac{|n|(n^2 - 1)}{\text{Ca}} \\ & + b' \left\{ \frac{2 \cos \beta}{R(t)\delta} \frac{|n|}{\text{Ca}} \mp \frac{R(t)\delta}{b_i^2(t)} \right. \\ & + \left. \frac{3|n|}{(1 + 2|n|)} \frac{\Phi_2}{\Phi_1} \left[\frac{b_i(t)}{[R(t)\delta]^2} \frac{(n^2 - 1)}{\text{Ca}} \mp \frac{R(t)\delta}{2b_i^2(t)} \right] \right\} \\ & - b'^2 \left\{ \frac{3|n|}{(1 + 2|n|)} \frac{\Phi_2}{\Phi_1} \frac{2 \cos \beta}{b_i(t)} \frac{1}{\text{Ca}} \right\} \end{aligned} \quad (16)$$

is the time-dependent linear growth rate $\lambda(n) = \lambda(n,t)$ and $\text{Ca} = 12\eta|\dot{b}|/\sigma$ is the capillary number. The upper signs appearing in Eq. (16) are related to the lifting flow, and the lower signs are related to squeeze flow. Equation (16) is a central result of this work, yielding explicit dependence of mode growth rates on b' , δ , Ca , and mode number n . Notice that when $b' = 0$, Eq. (16) reproduces the simpler results originally obtained in Ref. [4] for the corresponding lifting problem with parallel Hele-Shaw cell plates. As will become clear in Sec. III, the interplay of the parameters b' , δ , and Ca is a fundamental asset to allow the control and tuning of the fingering instability.

III. CONTROL OF THE FINGERING INSTABILITY

In this section we use the linear dispersion relation (16) to investigate how the depth gradient can be utilized to either restrain or promote the formation of interfacial viscous fingering structures in variable-gap Hele-Shaw flows. We do this by making sure that the values of the relevant dimensionless quantities we choose are consistent with realistic physical quantities related to existing experimental arrangements in lifting and squeeze parallel plate flows and material properties of the fluids [4–35].

A. Lifting flow

First, we examine the lifting Hele-Shaw flow, which is unstable in the limit of a parallel plates cell. Figure 2 plots

the linear growth rate $\lambda(n)$ as a function of the mode number n at $t = 0$ for positive [Fig. 2(a)] and negative [Fig. 2(b)] values of the gap gradient b' , as well as for the case $b' = 0$. The choice of $t = 0$ is justified by the fact that in the lifting case the most unstable situation happens at the beginning of the process. In fact, by managing to suppress fingering at $t = 0$, one would ensure its inhibition at $t > 0$. We consider $Ca = 1.1 \times 10^{-4}$ and the aspect ratio $\delta = 250$. From Fig. 2(a) we readily see a large band of Fourier modes with $\lambda(n) > 0$, indicating, as expected, that the system is unstable under the usual parallel plate lifting arrangement ($b' = 0$, dashed curve). Figure 2(a) also illustrates that the introduction of a small positive gap gradient ($b' = 0.002$, gray curve) tends to stabilize the system with respect to the $b' = 0$ case: the band of unstable modes and the growth rate magnitudes are decreased.

Since for the lifting Hele-Shaw flow we wish to stabilize the interface as much as we can, we proceed by increasing the value of the gap gradient. By doing this, eventually a critical value of b' (defined as b'_c) is reached, such that the interfacial instability is strongly restrained. It is clear from Fig. 2(a) that the transition from an unstable to a stable situation occurs if both of the following conditions are met:

$$\lambda(n)|_{t=0} = 0, \quad \frac{\partial \lambda(n)}{\partial n}|_{t=0} = 0. \quad (17)$$

This defines a critical gap gradient at which the exchange of stability takes place. From Eq. (16) we have verified that the interfacial instability is enhanced if we consider that $\Phi_2/\Phi_1 = 1$, which is the upper bound value for the ratio Φ_2/Φ_1 . This is a convenient limit since it allows easy access to b'_c . Figure 2(a) shows that the addition of a tiny gradient in the cell depth ($b'_c = 0.0039$) is able to inhibit the emergence of viscous fingering in lifting Hele-Shaw flows.

Figure 2(b) plots $\lambda(n)$ as a function of n for $b' = 0$ (dashed curve) and $b' = -0.0017$ (gray curve) at $t = 0$. It is interesting to note that for a significantly small negative value of the gap gradient ($b' = -0.0017$) the interface becomes fairly more unstable compared with the parallel plates situation ($b' = 0$). The efficacy of the taper-induced controlling process is even more clearly illustrated in Fig. 3, where we plot linear simulations for the physical situations discussed in Fig. 2.

Figure 4 illustrates the variation of the critical gap gradient b'_c as the capillary number Ca is changed for three values of the aspect ratio: $\delta = 150, 200$, and 250 . In this plot, for a given value of δ , the region above (below) the curve corresponds

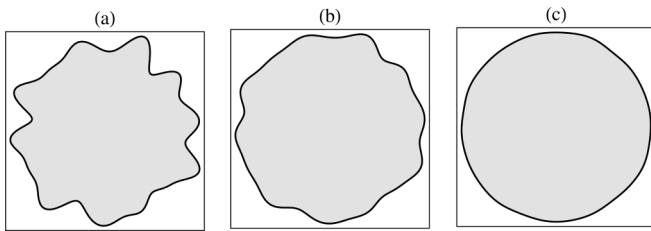


FIG. 3. Snapshot of the lifting interfacial patterns at time $t = 0.7$ for (a) a small negative gap gradient ($b' = -0.0017$), (b) parallel plates ($b' = 0$), and (c) the critical gap gradient ($b'_c = 0.0039$). These linear simulations include 40 Fourier modes and the same random choice of phases. The viscous fluid is depicted in gray. These resulting interfaces refer to the situations shown in Fig. 2.

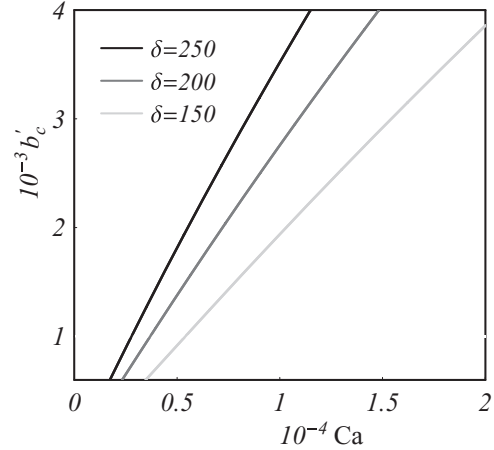


FIG. 4. Critical gap gradient b'_c as a function of the capillary number Ca for three values of δ : 150, 200, and 250. This graph works like a “phase diagram” for stability of the interface.

to a stable (unstable) situation. It is evident that in order to eliminate any interface deformation, higher values of b'_c are required as Ca is increased. Moreover, we also verify that for larger values of the aspect ratio, higher values of b' are needed to stabilize the interface. So a proper tuning of the parameters b' , Ca , and δ enables one to regulate the usual lifting instability which occurs when $b' = 0$ [4–17].

B. Squeeze flow

In this section we analyze the situation in which the upper plate is compressed against the lower one. Figure 5 plots $\lambda(n)$ at $t = 0$ as a function of n for three values of b' . As expected, we see that the usual parallel plate situation ($b' = 0$, dashed curve) is indeed stable [$\lambda(n) \leq 0$ for $n > 0$] since here the more viscous fluid pushes an inviscid fluid. However, we can destabilize the system by adding a small negative gap gradient. In Fig. 5 we identify unstable situations for $b' = -0.004$ (light gray curve) and for $b' = -0.006$ (dark gray curve). All these

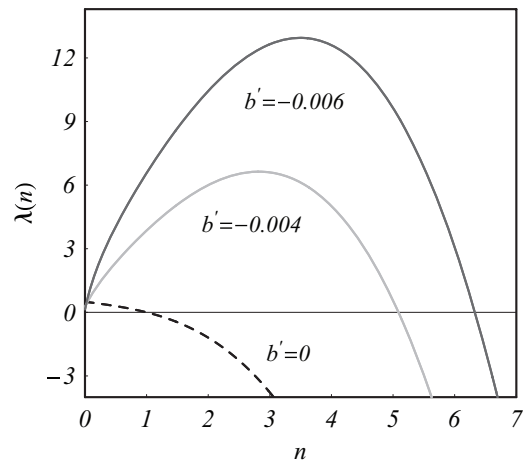


FIG. 5. Linear growth rate $\lambda(n)$ as a function of n for $Ca = 4 \times 10^{-5}$ and $\delta = 60$: $b' = 0$ (dashed curve), $b' = -0.004$ (light gray curve), and $b' = -0.006$ (dark gray curve).

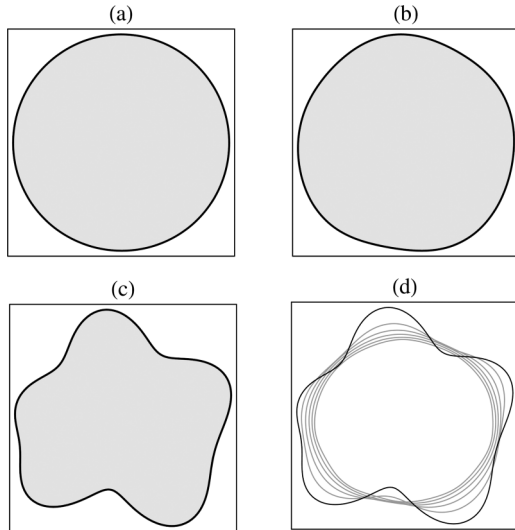


FIG. 6. Snapshot of the squeeze flow interfacial patterns at time $t = 0.27$ for (a) parallel plates ($b' = 0$), (b) a small gap gradient ($b' = -0.004$), and (c) a slightly larger gradient gap ($b' = -0.006$). (d) A sequence showing time development ($0 \leq t \leq 0.27$) leading to the interface shown in Fig. 6(c). These linear simulations include ten Fourier modes and the same random choice of phases. The viscous fluid is represented in gray. These resulting interfaces refer to the situations shown in Fig. 5.

facts are reinforced by the corresponding linear simulations depicted in Fig. 6.

Note that the small taper $b' < 0$ [Figs. 6(c) and 6(d)] furnishes an efficient way to induce interfacial destabilization and finger production for an originally stable squeeze flow situation (where $b' = 0$). It is worthwhile to note that destabilization for reverse fingering during squeeze flow has been recently observed experimentally [46], where the compression of a non-Newtonian starch gel leads to an interesting oscillatory behavior at the sample's interface. Incidentally, reverse flow destabilization has also been experimentally detected in rectangular Hele-Shaw flows [47] where the presence of a preexisting wetting layer of surfactant generates the development of fingering patterns with blunted fronts and sharp trailing tails. Other experiments, performed in the radial Hele-Shaw setup with particulate suspensions [48], exhibited unstable reserve flow induced by the effectively less viscous trailing suspension.

Since the growth rate (16) varies with time, to estimate the resulting number of fingers at a time t of the squeeze process we have to obtain the Fourier mode n_{\max} that maximizes the amplitude $\zeta_n(t)$. By inspecting Eq. (15), we easily see that the solution for $\zeta_n(t)$ is given by

$$\zeta_n(t) = \zeta_n(0) \exp \left[\int_0^t \lambda(n, t') dt' \right]. \quad (18)$$

The number of fingers at the interface is obtained by searching for the mode that maximizes the integral appearing in Eq. (18). Figure 7 plots n_{\max} as a function of b' for $\text{Ca} = 4 \times 10^{-5}$, $\delta = 60$ and 100. Note that larger negative values of b' are needed to obtain higher values of n_{\max} . On the other hand,

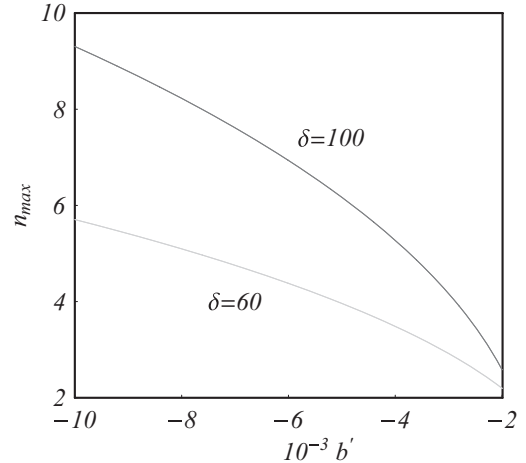


FIG. 7. The Fourier mode that maximizes the perturbation amplitude $\zeta_n(t)$ at $t = 0.3$ (n_{\max}) as a function of the gap gradient b' for $\text{Ca} = 4 \times 10^{-5}$ and two values of δ : 60 (light gray curve) and 100 (dark gray curve).

larger values of δ favor an increasingly larger production of fingers. So the tuning of the small gap gradient b' and of the aspect ratio δ serves not only to destabilize an originally stable situation but also to enable one to conveniently set the number of emerging interfacial fingers.

IV. CONCLUDING REMARKS

A modification of the traditional variable-gap Hele-Shaw cell setup in which a gradient in the flow passage is introduced has been proposed. The suggested modified arrangement allows both lifting and squeezing flows to take place and offers the possibility of investigating the influence of the small depth gradient on the development of interfacial fingering instabilities.

By appropriately generalizing the basic equations of the system, in particular the continuity equation and the Young-Laplace pressure jump condition, a linear dispersion relation is derived. We have shown that the linear behavior of the system can be conveniently described in terms of three dimensionless parameters, namely, the depth gradient b' , the capillary number Ca , and the aspect ratio δ . By tuning these parameters we have found that the consideration of the tapered Hele-Shaw geometry fundamentally changes the stability of the fluid-fluid interface. Specifically, we have identified a taper-induced controlling strategy permitting the restraining of fingering in lifting flows, as well as the triggering of interfacial disturbances in squeeze flows. These results might provide a useful starting point for the design of a taper-regulated debonding process of fluid materials in adhesion related problems [13,17,22].

ACKNOWLEDGMENTS

We thank CNPq for financial support through the program “Instituto Nacional de Ciência e Tecnologia de Fluidos Complexos (INCT-FCx)” and FACEPE through PRONEM Project No. APQ-1415-1.05/10.

- [1] P. G. Saffman and G. I. Taylor, *Proc. R. Soc. London, Ser. A* **245**, 312 (1958).
- [2] G. M. Homsy, *Annu. Rev. Fluid Mech.* **19**, 271 (1987); K. V. McCloud and J. V. Maher, *Phys. Rep.* **260**, 139 (1995).
- [3] L. Paterson, *J. Fluid Mech.* **113**, 513 (1981).
- [4] M. J. Shelley, F.-R. Tian, and K. Wlodarski, *Nonlinearity* **10**, 1471 (1997).
- [5] J. Bohr, S. Brunak, and T. Nørretranders, *Europhys. Lett.* **25**, 245 (1994).
- [6] S. Roy and S. Tarafdar, *Phys. Rev. E* **54**, 6495 (1996).
- [7] S. K. Thamida, P. V. Takhistov, and H.-C. Chang, *Phys. Fluids* **13**, 2190 (2001).
- [8] S. Sinha, S. K. Kabiraj, T. Dutta, and S. Tarafdar, *Eur. Phys. J. B* **36**, 297 (2003).
- [9] S. K. Kabiraj and S. Tarafdar, *Phys. A* **328**, 305 (2003).
- [10] J. A. Miranda and R. M. Oliveira, *Phys. Rev. E* **69**, 066312 (2004).
- [11] C.-Y. Chen, C.-H. Chen, and J. A. Miranda, *Phys. Rev. E* **71**, 056304 (2005).
- [12] M. Ben Amar and D. Bonn, *Phys. D* **209**, 1 (2005).
- [13] A. Lindner, D. Derks, and M. J. Shelley, *Phys. Fluids* **17**, 072107 (2005).
- [14] J. Nase, A. Lindner, and C. Creton, *Phys. Rev. Lett.* **101**, 074503 (2008).
- [15] S. Sinha, T. Dutta, and S. Tarafdar, *Eur. Phys. J. E* **25**, 267 (2008).
- [16] E. O. Dias and J. A. Miranda, *Phys. Rev. E* **81**, 016312 (2010).
- [17] J. Nase, D. Derks, and A. Lindner, *Phys. Fluids* **23**, 123101 (2011).
- [18] J. Engmann, C. Servais, and A. S. Burbidge, *J. Non-Newtonian Fluid Mech.* **132**, 1 (2005).
- [19] R. B. Bird, R. Armstrong, and O. Hassager, *Dynamics of Polymeric Liquids* (Wiley, New York, 1977).
- [20] B. A. Francis and R. G. Horn, *J. Appl. Phys.* **89**, 4167 (2005).
- [21] D. Derks, A. Lindner, C. Creton, and D. Bonn, *J. Appl. Phys.* **93**, 1557 (2003).
- [22] S. Poivet, F. Nallet, C. Gay, and P. Fabre, *Europhys. Lett.* **62**, 244 (2003).
- [23] M. Tirumkudulu, W. B. Russel, and T. J. Huang, *Phys. Fluids* **15**, 1588 (2003).
- [24] R. D. Welsh, M.Sc. thesis, Massachusetts Institute of Technology, 2001.
- [25] J. A. Miranda, *Phys. Rev. E* **69**, 016311 (2004).
- [26] J. A. Miranda, R. M. Oliveira, and D. P. Jackson, *Phys. Rev. E* **70**, 036311 (2004).
- [27] S. Poivet, F. Nallet, C. Gay, J. Teisseire, and P. Fabre, *Eur. Phys. J. E* **15**, 97 (2004).
- [28] Y. O. M. Abdelhay, M. Chaouche, and H. Van Damme, *Appl. Clay Sci.* **42**, 163 (2008).
- [29] S. A. Lira and J. A. Miranda, *Phys. Rev. E* **80**, 046313 (2009).
- [30] Q. Barral, G. Ovarlez, X. Chateau, J. Boujlel, B. Rabideau, and P. Coussot, *Soft Matter* **6**, 1343 (2010).
- [31] R. H. Ewoldt, P. Tourkine, G. H. McKinley, and A. E. Hosoi, *Phys. Fluids* **23**, 073104 (2011).
- [32] E. O. Dias and J. A. Miranda, *Phys. Rev. E* **85**, 016312 (2012).
- [33] E. O. Dias and J. A. Miranda, *Phys. Rev. E* **86**, 046322 (2012).
- [34] A. Zosel, *Colloid Polym. Sci.* **263**, 541 (1985).
- [35] H. Lakrout, P. Sergot, and C. Creton, *J. Adhes.* **69**, 307 (1999).
- [36] H. Zhao, J. Casademunt, C. Yeung, and J. V. Maher, *Phys. Rev. A* **45**, 2455 (1992); *Phys. Rev. E* **48**, 1601 (1993).
- [37] E. O. Dias and J. A. Miranda, *Phys. Rev. E* **82**, 056319 (2010).
- [38] T. T. Al-Housseiny, P. A. Tsai, and H. A. Stone, *Nat. Phys.* **8**, 747 (2012).
- [39] R. M. Wilson, *Phys. Today* **65**(10), 15 (2012).
- [40] A. Juel, *Nat. Phys.* **8**, 706 (2012).
- [41] T. T. Al-Housseiny and H. A. Stone, *Phys. Fluids* (accepted).
- [42] E. O. Dias and J. A. Miranda, *Phys. Rev. E* **87**, 053014 (2013).
- [43] S.-Z. Zhang, E. Louis, O. Pla, and F. Guinea, *Eur. Phys. J. B* **1**, 123 (1998).
- [44] I. S. Gradshteyn and I. M. Ryzhik, *Table of Integrals, Series, and Products* (Academic, New York, 1994).
- [45] M. Abramowitz and I. A. Stegun, *Handbook of Mathematical Functions with Formulas, Graphs, and Mathematical Tables* (Dover, New York, 1972).
- [46] M. Dutta Choudhury, S. Chandra, S. Nag, S. Das, and S. Tarafdar, *Colloids Surf. A* **407**, 64 (2012).
- [47] C. K. Chan and N. Y. Liang, *Phys. Rev. Lett.* **79**, 4381 (1997).
- [48] H. Tang, W. Grivas, D. Homentcovschi, J. Geer, and T. Singler, *Phys. Rev. Lett.* **85**, 2112 (2000).